2D Materials

OPEN ACCESS

RECEIVED
26 March 2015

REVISED
18 June 2015

ACCEPTED FOR PUBLICATION
2 July 2015

PUBLISHED
30 July 2015

PAPER

Photoluminescence of two-dimensional GaTe and GaSe films

O Del Pozo-Zamudio[1], S Schwarz[1], M Sich[1], I A Akimov[2], M Bayer[2], R C Schofield[1], E A Chekhovich[1], B J Robinson[3], N D Kay[3], O V Kolosov[3], A I Dmitriev[4], G V Lashkarev[4], D N Borisenko[5], N N Kolesnikov[5] and A I Tartakovskii[1,1]

[1] Department of Physics and Astronomy, University of Sheffield, Sheffield S3 7RH, UK
[2] Experimentelle Physik 2, Technische Universität Dortmund, 44227 Dortmund, Germany
[3] Department of Physics, University of Lancaster, Lancaster LA1 4YB, UK
[4] I. M. Frantsevich Institute for Problems of Material Science, NASU, Kiev-142, Ukraine
[5] Institute of Solid State Physics, Russian Academy of Sciences, Chernogolovka 142432, Russia

E-mail: o.delpozo@sheffield.ac.uk **and** a.tartakovskii@sheffield.ac.uk

Keywords: 2D semiconductors, III-VI materials, optical properties, photoluminescence

Supplementary material for this article is available online

Abstract

Gallium chalcogenides are promising building blocks for novel van der Waals heterostructures. We report on the low-temperature micro-photoluminescence (PL) of GaTe and GaSe films with thicknesses ranging from 200 nm to a single unit cell. In both materials, PL shows a dramatic decrease by 10^4–10^5 when film thickness is reduced from 200 to 10 nm. Based on evidence from continuous-wave (cw) and time-resolved PL, we propose a model explaining the PL decrease as a result of non-radiative carrier escape via surface states. Our results emphasize the need for special passivation of two-dimensional films for optoelectronic applications.

1. Introduction

The discovery and research of the remarkable properties of two-dimensional (2D) sheets of carbon [1], known as graphene, has sparked interest in other layered materials such as metal chalcogenides (MCs) [2, 3]. Recent progress in device fabrication opens up new possibilities for 2D MC films in nano- and optoelectronics [3–8]. Recent efforts in the research of 2D semiconductors and their devices focused mainly on molybdenum and tungsten dichalcogenides [4, 8–13] and relatively little has been reported on the optical properties of thin films of III–VI materials: only recently electronic [4, 14–16] and photonic [17] trial devices have been reported for GaSe and GaTe [16], and room-temperature photoluminescence (PL) was measured in detail for InSe thin films [18]. As the crystal growth and improvement of thin GaSe films continues [14, 19, 20], further exploration of the physical properties of III–VI materials presented in this work is motivated by their potential use as building blocks for novel van der Waals heterostructures, where materials with a range of bandgaps and band offsets will be required [5, 8]. Furthermore, in contrast to molybdenum and tungsten chalcogenides emitting light efficiently only in films with a single unit cell thickness, III–VI materials are bright light emitters in a range of thicknesses [18]. This may relax the stringent fabrication requirements and add flexibility for novel heterostructured devices such as light emitting diodes [8].

Both GaTe and GaSe are layered crystals with strong covalent in-plane inter-atomic bonding (with some ionic contributions [21, 22]) and weaker predominantly van der Waals inter-plane bonding [21, 23–26]. A single tetralayer with a hexagonal in-plane structure consists of two Ga atoms and two Se or Te atoms: Se–Ga–Ga–Se and Te–Ga–Ga–Te [25]. The bulk lattices are built by stacking tetralayers, which can occur in several ways [21, 23, 24]. For the wider studied GaSe, several types of stacking exist leading to different polytypes [21, 23, 24]. For GaTe with a monoclinic crystal lattice [22, 27] the polytypic behavior has not been observed [22, 26]. This may lead to a lower probability of stacking faults in GaTe, resulting in clearer observation (compared to GaSe) of excitonic features in optical experiments [22, 26].

Here we study the optical properties of GaSe and GaTe thin films as a function of the film thickness. Continuous-wave (cw) and time-resolved low-

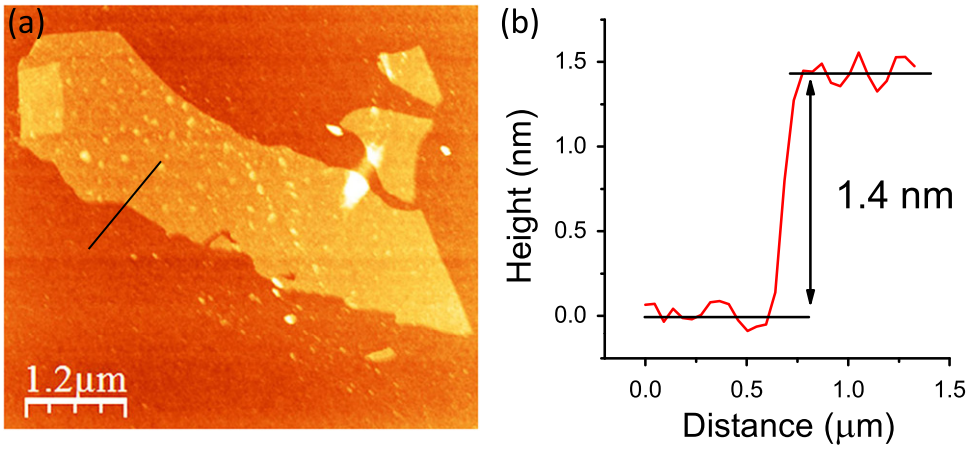

Figure 1. (a) AFM image of a GaSe thin film with a single unit cell thickness. This film was obtained by mechanical exfoliation. (b) Cross-sectional plot along the black line in (a).

temperature micro-PL for a wide range of films from 200 nm to one tetralayer thicknesses is measured. PL intensity is used to monitor the quantum yield (QY), which falls dramatically for thin films: integrated cw PL intensity drops by up to $\approx 10^4$–10^5 when the film thickness is reduced from 200 to 10 nm. A similar observation of reduced PL for thin films was previously reported for InSe and was explained as the transition to a band-structure with an indirect bandgap, the conclusion also based on the observed PL blue-shift with the decreasing film thickness [18]. Such indirect bandgap behavior is also theoretically predicted for single monolayers of GaSe and GaTe [25]. However, no size-quantization effects as in InSe are observed in our work for GaSe and GaTe. Based on the evidence from both cw and time-resolved spectroscopy, we develop a model that shows that the observed PL reduction can be explained by non-radiative carrier escape to surface states. Our explanation does not require introduction of the direct-to-indirect band-gap transition. Following the cw PL data analysis, we identify a critical film thickness of about 30–40 nm, below which the non-radiative carrier escape changes its character. The importance of surface states predicted by our results emphasizes the need for development of novel surface passivation for III–VI films, possibly involving oxygen-free dielectrics such as boron nitride [28].

2. Experimental procedure

2.1. Fabrication of GaTe and GaSe samples

Single crystals of GaSe and GaTe were grown by high-pressure vertical zone melting in graphite crucibles under Ar pressure. A detailed description of the crystal growth processes and properties of GaSe and GaTe can be found in [29–32]. The gallium mono-chalcogenides used in this work were synthesized from high-purity materials: Ga and Te–99.9999%, Se–99.9995%. The crystals used are high-resistivity semiconductors with low free carrier absorption, which has been confirmed in infra-red transmission measurements. GaSe and GaTe have n-type and p-type conductivity, respectively. This is a typical observation: selenides are usually of n-type conductivity, whereas tellurides can often have conductivity of both types, even within one ingot. Such behavior is attributed to deviations of the crystal composition from stoichiometry, usual for metal chalcogenides. In our case the n-type conductivity clearly indicates some excess of Ga (donor) in GaSe, whereas the p-type conductivity indicates a slight excess of Te (acceptor) in the GaTe.

The III–VI thin films studied in this work were fabricated by mechanical cleaving from bulk. The films were deposited on Si/SiO_2 substrates. Within the first 15 minutes after the exfoliation/deposition procedure, the films were placed in a plasma-enhanced chemical vapor deposition (PECVD) reactor and a 15 nm Si_3N_4 layer was deposited with the sample maintained at a temperature of 300 °C. This process leads to a complete encapsulation of the films, protecting them from interaction with oxygen and water present in the atmosphere. We carried out comparative PL studies with uncapped samples, which showed no effect on the optical properties of dielectric deposition and heating the sample to a few hundred degrees. In our experiments the capping is necessary because both materials (particularly GaSe) are unstable in air. Films with a wide variety of thicknesses were obtained from a single unit cell (single monolayer, ML) shown in figure 1 to 200 nm. The thicknesses of the films were determined using atomic force microscopy in a Veeco Dimension 3100 microscope, where films were measured in a tapping mode in ambient conditions.

2.2. Optical characterization methods

Optical characterization of the GaTe and GaSe thin films was carried out using a low-temperature micro-photoluminescence (μPL) technique. The sample was

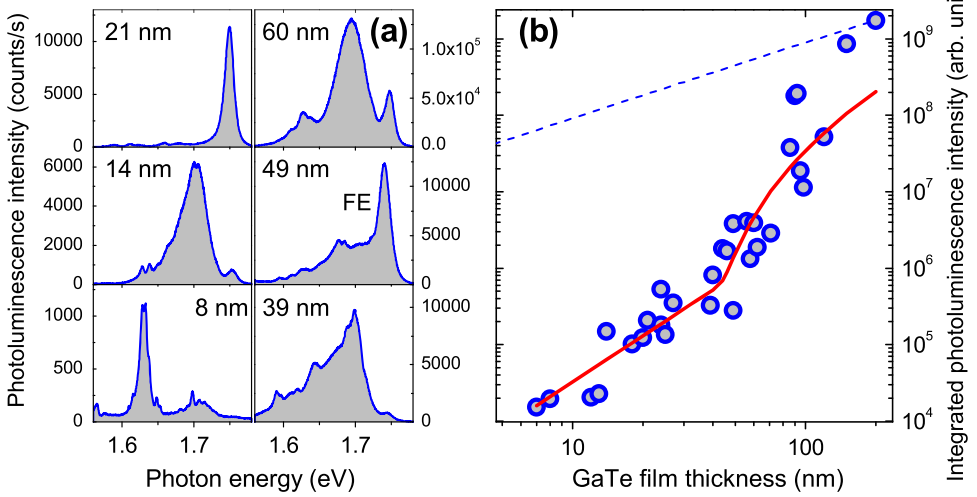

Figure 2. Low-temperature cw PL results for GaTe thin films. (a) PL spectra for films of various thicknesses. h_{film} is marked on the plots. On the plot for the film with $h_{film} = 49$ nm FE marks the free exciton peak observed at similar energies for all films on the figure except the one with $h_{film} = 8$ nm. (b) Symbols show experimentally measured integrated PL (for $T = 10$ K) for the cw laser excitation power of 2 mW at 532 nm (2.33 eV). The dashed line shows expected variation of PL following the change in the absorption of the thin film assuming constant quantum efficiency. The solid line shows the results of calculations using the model discussed in the text.

placed on a cold finger in a continuous flow He cryostat at a temperature of 10 K. A microscope objective with a numerical aperture (NA) of 0.6 was placed outside the cryostat and was used to focus the laser beam on the sample (in a ≈2 μm spot) and to collect the PL from the films. In cw experiments, PL was detected with a 0.5 m spectrometer and a liquid nitrogen cooled charge coupled device. For cw PL excitation a laser emitting at 532 nm (2.33 eV) was used. In the ultra-fast spectroscopy experiments the excitation of GaTe and GaSe layers was performed using frequency-doubled titanium-sapphire (wavelength of 415 nm, pulse duration ≈200 fs) focused on the sample in an ≈10 μm spot. Time-resolved PL (TRPL) was detected using a streak camera. The temporal resolution of the experimental setup for the time-resolved measurements was 10 ps.

3. Experimental results

3.1. Low-temperature cw PL results: GaTe

Figure 2(a) shows typical PL spectra measured for Si_3N_4-capped GaTe thin films at $T = 10$ K (cw laser power $P = 2$ mW in figure 2(a)). In this figure, in all films but the one with a thickness $h_{film} = 8$ nm, a narrow feature is observed around 1.75 eV. It is observed at an energy where free exciton (FE) PL is expected. We will therefore refer to such features in GaTe (and GaSe) films as a 'free exciton' peak as opposed to the low energy broad PL bands corresponding to excitons bound to impurities/defects and observed in the range of 1.6–1.7 eV for GaTe. The 'free excitons' may also experience disordered potential and a degree of localization as evidenced from a relatively broad FE PL line of 10–15 meV (varying from sample-to-sample). A different behavior of the FE peak compared to the bound excitons has been verified in temperature and power-dependent measurements and is further confirmed in time-resolved studies discussed below. The FE peak is usually more pronounced in thick films of around 100 nm and above. In thin films, as in the 8 nm film in the figure, the FE peak could only be observed under high power pulsed excitation, when the impurity/defect states saturate. The sharpest PL feature in GaTe spectra, the FE line, has a peak energy varying from film to film in the range 1.74–1.76 eV showing the insignificance of size-quantization effects in contrast to InSe where the PL blue-shift was observed for thin layers [18].

A pronounced feature of PL measured from different films is a dramatic decrease of PL intensity with the decreasing thickness of the material (see figure 2(b)): about 10^5 (10^4) decrease is observed between 200 (100) and 7 nm. The strongest PL reduction by three orders of magnitude is detected between 200 and 40 nm. For $h_{film} < 40$ nm, the PL intensity reduction slows down and decreases less than 100 times when h_{film} is varied between 40 and 7 nm. The dotted curve in the graph shows the expected PL intensity behavior assuming thickness-independent quantum efficiency, i.e. when reduction in PL is caused solely by the reduced absorption and reduced number of e–h pairs created by the laser. The curve is described by the expression $I_{PL} = I_{GaTe}[1 - \exp(-\alpha_{GaTe} h_{film})]$, where I_{GaTe} is the PL intensity for films with $h_{film} \approx 200$ nm. The absorption coefficient $\alpha_{GaTe} = 5000$ cm^{-1} is used according to [33]. A discrepancy of a few orders of magnitude between the experiment and the calculated curve in a wide range of film thicknesses is evident on the graph. The strong deviation

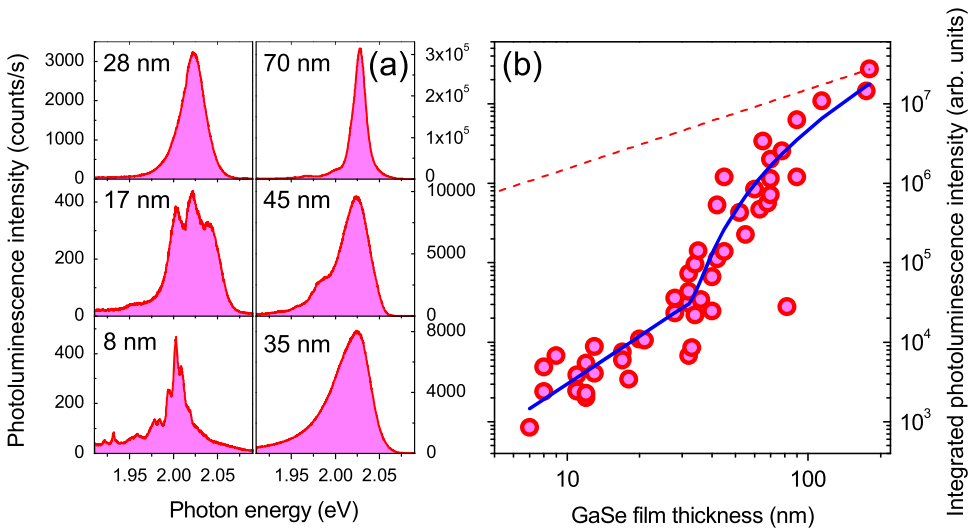

Figure 3. Low-temperature cw PL results for GaSe thin films. (a) PL spectra for films of various thicknesses. (b) Symbols show experimentally measured integrated PL (for $T = 10$ K) for the cw laser excitation power of 2 mW at 532 nm (2.33 eV). The dashed line shows expected variation of PL following the change in the absorption of the thin film assuming constant quantum efficiency. The solid line shows the results of calculations using the model discussed in the text.

from the calculated curve signifies a strong decrease of the quantum efficiency with decreasing film thickness.

3.2. Low-temperature cw PL results: GaSe

Figure 3(a) shows typical PL spectra measured for Si_3N_4-capped films of GaSe of several thicknesses between 8 and 70 nm (a cw laser power of 2 mW is used). The PL signal is observed in a range from 1.95–2.05 eV, which is below the emission energy of the free exciton, reported to be around 2.10 eV for some high purity GaSe samples (see e.g. [34]). The detected PL in our samples thus comes from impurity/defect states. The observed localized states may originate from the non-stoichiometric composition of the bulk material.

In figure 3(a) it is observed that the PL spectra of thin films <20 nm usually consist of multiple pronounced lines (a feature similar to GaTe in figure 2(a)), whereas PL spectra tend to exhibit a single pronounced peak for thicker films. PL linewidths vary between 15 and 60 meV. In some GaSe films, sharp PL lines with linewidths below 5 meV, similar to the sharp features observed in the PL spectrum for the 8 nm film in figure 3(a), also occur in the whole energy range of GaSe PL. From the data measured on more than 50 films, we observe that PL peak energies have a very wide distribution in the range 1.99–2.06 eV. Similarly to GaTe, there is no evidence for size-quantization effects as a function of the film thickness.

Further evidence for exciton localization in thin films is a pronounced Stokes blue-shift observed when the laser excitation density is increased as shown in figure 4. The inset in figure 4(a) shows that the PL peak shifts by ≈20 meV as the cw laser power is changed from 0.01 to 2 mW. This is a typical behavior observed in all GaSe films independent of the film thickness: at high power, saturation of some of the PL features is observed accompanied in most cases with a blue-shift of PL of around 10–20 meV. This is a typical behavior observed for localized exciton states in semiconductors, an effect also similar to the state-filling phenomenon in semiconductor quantum dots [35].

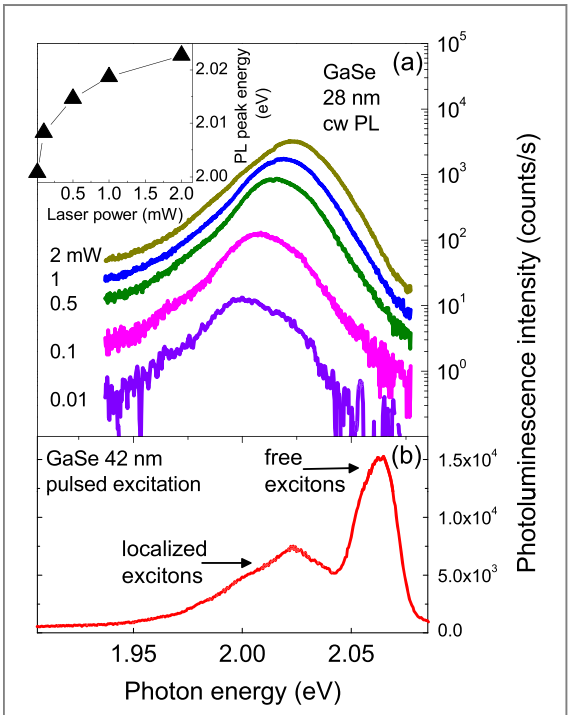

Figure 4. (a) Observation of the Stokes shift of localized exciton states in cw PL of a 28 nm thick GaSe films. Excitation with a cw laser at 532 nm (2.33 eV) is used at $T = 10$ K. (b) Observation of the free exciton feature in PL of a 42 nm thick GaSe film. The time-integrated PL is shown measured for pulsed laser excitation at 420 nm (2.95 eV) with a power of 1 mW. A free exciton peak with a linewidth of ≈25 meV is observed at 2.06 eV.

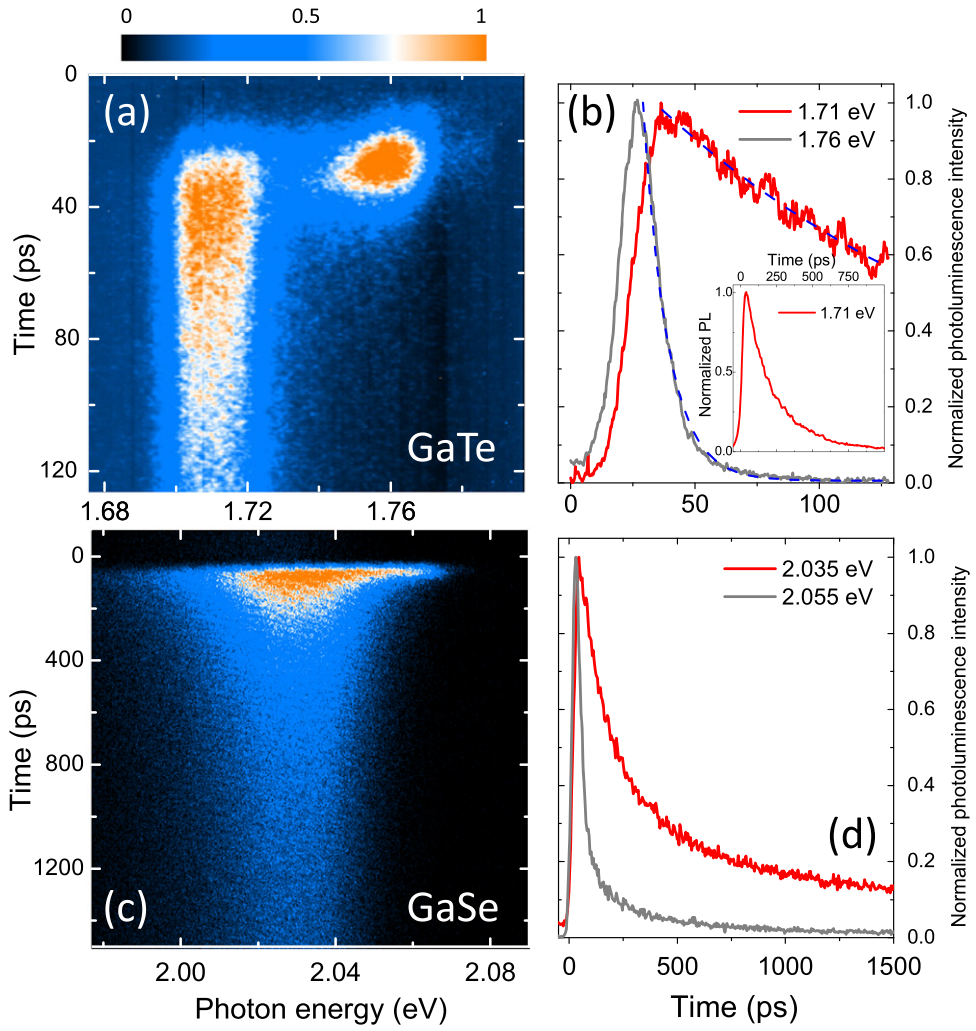

Figure 5. Time-resolved PL data for GaTe (a), (b) and GaSe (c), (d) thin films measured at $T = 10$ K. Note the different time-scales for the GaTe and GaSe data. (a), (c) Streak-camera scans. (b), (d) PL traces measured at 1.76 (gray) and 1.71 eV (red) for GaTe and 2.055 (gray) and 2.035 eV (red) for GaSe. The blue lines in (b) show fitting with a single exponential function as described in the text.

In some GaSe films, if the optical pumping is further increased, for example, by using pulsed excitation, a relatively broad free exciton feature can be observed, as shown in figure 4(b). This behavior is in agreement with that observed previously in GaTe and GaSe under pulsed excitation, and is related to saturation of the localized states with relatively slow recombination rates [36].

Similarly to GaTe films, a significant decrease of PL intensity with the decreasing thickness of the GaSe films is observed (see figure 3(b)) by about 2×10^4 between 200 and 7 nm. As for the GaTe films in figure 2(b), the strongest PL reduction by three orders of magnitude is detected between 200 and 30 nm. For $h_{\text{film}} < 30$ nm, the PL intensity reduction slows down and is about 30 when h_{film} is varied between 30 and 7 nm. Similar to GaTe in films with $h_{\text{film}} < 7$ nm PL is completely suppressed. Similarly to figure 2, we show a curve that describes PL reduction due to the reduced absorption only calculated as $I_{\text{PL}} = I_{\text{GaSe}}[1 - \exp(-\alpha_{\text{GaSe}} h_{\text{film}})]$, where I_{GaSe} is the PL intensity for films with $h_{\text{film}} = 150$ nm and the absorption coefficient $\alpha = 1000\,\text{cm}^{-1}$ [33]. As for GaTe, a significant discrepancy by a few orders of magnitude between the experimental results and the calculated curve is clear in a wide range of film thicknesses, indicating a strong decrease of the quantum efficiency with decreasing film thickness.

3.3. Time-resolved PL measurements

In order to shed further light on the results of cw PL and also to provide a further experimental foundation for our theoretical model, time-resolved PL experiments have been carried out for a range of films with different thicknesses. Figure 5 shows typical TRPL data obtained at $T \approx 10$ K.

For GaTe, the difference in the origin of the PL features observed in figure 2(a) is further evidenced in TRPL. Figures 5(a), (b) shows data for a 27 nm thick film exhibiting a behavior typical for films with h_{film} in the range 20–200 nm. Figure 5(a) presents a streak-camera scan clearly showing two pronounced features at 1.76 eV and 1.71 eV corresponding to the free and localized excitons, respectively. The free exciton peak

intensity decays considerably faster than that of the localized states, which does not change significantly on the time-scale of 130 ps shown in the figure. Figure 5(b) shows two decay curves measured at 1.76 eV (gray) and 1.71 eV (red). Fitting with single exponential decay functions is shown with blue curves and gives 10 ps for the free exciton and 150 ps for the localized states. The inset shows a PL decay curve measured at 1.71 eV on a larger time-scale, exhibiting an almost complete decay of the signal at 1 ns. We find similar life-times for other films, however no clear dependence on the film thickness is observed: the free exciton PL decay time varies between 5 and 25 ps and that for the localized states between 100 and 200 ps. The lifetimes also weakly depend on the laser excitation power. We also note the rise times of ≈15 and 20 ps for the free and localized states, respectively, indicating fast carrier relaxation into the light-emitting states.

A similar difference between the PL dynamics of the high and low energy part of the spectrum is observed for GaSe thin films in figure 5(c), (d). Here a behavior resembling the Stokes shift shown in figure 4 is observed: as the carrier density decreases with time after the laser pulse, the PL intensity maximum progressively moves to lower energy. Figure 5(d) details the behavior shown in figure 5(c): two decay curves measured at 2.055 eV (gray) and 2.035 eV (red) are shown. In the center of the PL band at 2.035 eV, the non-exponential decay occurs with a characteristic time of 400 ps, which also shows a slow-decaying component. At around 2.055 eV, the initial PL time-dependence can be well fitted with a single-exponential decay with a lifetime of ≈40 ps, dominated most likely by carrier relaxation to lower energy. The complex behavior in GaSe films occurs due to the partial saturation of the states at short times after the excitation pulse and fast relaxation to lower energy. We find similar behavior for films with other thicknesses. Similarly to GaTe no clear dependence on the film thickness is observed and the rise times of ≈30 ps are found for the localized states.

3.4. Modeling

In order to describe the observed trend of PL intensity as a function of film thickness h_{film} in GaSe and GaTe thin films we have developed a rate equation model presented in detail in the Supplementary Information [37]. As shown in figures 6(a), in the model we consider the following processes leading to light emission: optical excitation of e–h pairs (uniformly across the full thickness of the film); relaxation into the non-radiative traps with a time τ_{nr1} or τ_{nr2} depending on the thickness of the film, as explained below; relaxation with a time τ_{rel} into the light-emitting states denoted in figure 6(a) as 'PL states'; PL emission from these states with a time τ_{PL}. The absence of a clear dependence of the PL decay times on the film thickness allows us to use a thickness-independent constant τ_{PL} and neglect any other decay mechanisms for the e–h population of the light-emitting states. The physical origin of this may be in a relatively strong localization of e–h pairs in the light-emitting 'PL states', which leads to suppression of non-radiative processes. We also assume that the mechanism of relaxation into the 'PL states' is not sensitive to the film thickness and can be described with a thickness independent time τ_{rel}.

As shown in figures 6(b) and (c) we also assume that the film is divided into three regions: (1) two regions of thickness h_0 near the film surfaces where fast carrier relaxation to surface traps occurs leading to non-radiative carrier escape; (2) a 'normal' region of thickness $h_{film} - 2h_0$ in the film's central part not containing the traps where the photo-excited carriers can escape into regions (1), where they undergo non-radiative decay. Here the h_0 value may be associated with a depletion depth or an average surface trap radius [37]. As shown in figure 6 there are two possibilities: in figure 6(b), where $h_{film} > 2h_0$ and both regions of type (1) and (2) exist; and in figure 6(c), for films with $h_{film} \leqslant 2h_0$, where region (2) is not present. The model assumes that light absorption and PL occurs in both types of regions. In both regions, e–h pairs relax with the time τ_{rel} into the light-emitting states.

In region (1), in the first approximation the average time it takes for the carrier/e–h pair to escape non-radiatively is proportional to half the thickness of region (1) (can be understood as the average time for the carrier to reach the surface or as the overlap of the wavefunction of the carrier and the surface trap). In region (2), the non-radiative escape time reflects the average time it takes for a carrier or an e–h pair to reach any of the regions (1). The underlying mechanism for this process may be depletion and band-bending expected at the film surface leading to charge separation and non-radiative decay [37]. We assume that once the carrier or e–h pair has reached region (1) it escapes non-radiatively. In the first approximation, the average time it takes a carrier/e–h pair to reach region (1) is proportional to half the thickness of region (2). Thus we introduce non-radiative decay times in region (1) as $\tau_{nr1} = (h_0/2)/u_1$ for $h_{film} > 2h_0$, and $\tau_{nr1} = (h_{film}/4)/u_1$ for $h_{film} \leqslant 2h_0$. In region (2) it is $\tau_{nr2} = (h_{film}/2 - h_0)/u_2$. Here u_1 and u_2 have dimensions of m/s. In the case of region 2 where effectively we assume ballistic exciton (or electron/hole) transport preceding the non-radiative escape, u_2 can be interpreted as the average carrier velocity.

3.5. Discussion

As detailed in the supplementary data and observed in figures 2(b) and 3(b), we find that the proposed model provides a reasonable description of our data using four parameters (which are not completely

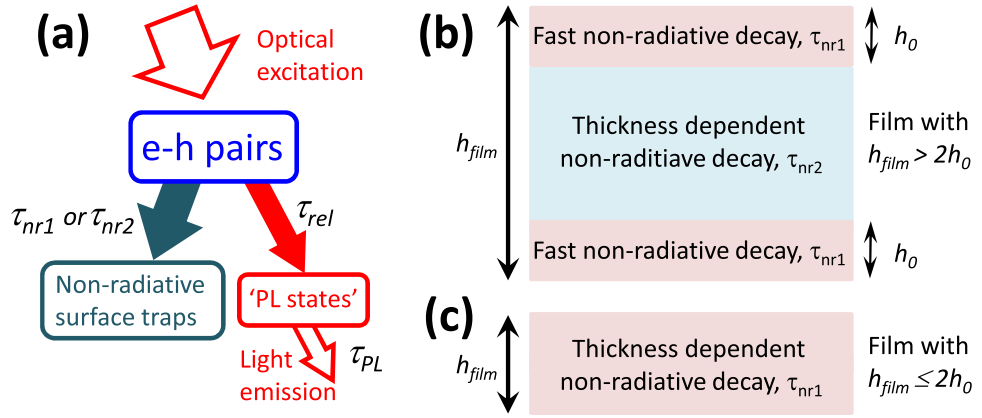

Figure 6. Diagrams illustrating the theoretical model for the dependence of the cw PL intensity on the film thickness. (a) Processes included in the model (see the text and the supplementary data for more details): optical excitation of e–h pairs; relaxation into the non-radiative traps with a time τ_{nr1} or τ_{nr2} depending on the thickness of the film; relaxation with a time τ_{rel} into the light-emitting states denoted as 'PL states'; PL emission from these states with a time τ_{PL}. (b), (c) Two types of thin films with thicknesses above and below the critical thickness of $2h_0$. In (b) we show a relatively thick film with a thickness of $h_{film} > 2h_0$. This film has three regions: two regions of thickness h_0 near the film surfaces where fast carrier relaxation to surface traps occurs (shown in pink), and a 'normal' region of thickness $h_{film} - 2h_0$ in the middle of the film (blue) where non-radiative processes are weaker and occur through carrier escape into the surface regions. In (c) we show a thin film with $h_{film} \leqslant 2h_0$, where a region of only one type exists, where fast non-radiative carrier decay occurs.

independent as we find): the 'critical' thickness h_0, a parameter describing the amount of light absorbed by the film, and products $\tau_{rel}u_1$ and $\tau_{rel}u_2$. In particular the fitting functions that we produce capture the change in the 'slope' of the data observed at around 30 nm for GaSe and 40 nm for GaTe, which we interpret as the thickness of the film where $h_{film} \approx 2h_0$, i.e. the thickness of region (2) turns to zero, and non-radiative carrier escape changes its character.

However, we find that the accuracy of the fitting is not sufficient to extend our analysis beyond determination of the order of magnitude of the products $\tau_{rel}u_1$ and $\tau_{rel}u_2$. We find that $\tau_{rel}u_1$ and $\tau_{rel}u_2$ are of the order of 1000 and 100 nm, respectively, for both GaSe and GaTe. The solid line shown in figure 2(b) for GaTe films is obtained for $\tau_{rel}u_1 = 3800$ nm and $\tau_{rel}u_2 = 200$ nm, whereas the fitting in figure 3(b) for GaSe films is done for $\tau_{rel}u_1 = 2900$ nm and $\tau_{rel}u_2 = 150$ nm. We note that the description of GaSe PL is more satisfactory, possibly because in GaTe there is a contribution from free exciton PL, so additional non-radiative escape channels and relaxation processes need to be taken into account. For thicker GaTe films, much stronger PL than predicted by the model is observed, which probably signifies suppression of additional non-radiative escape that free excitons experience in relatively thin films. It is also notable that in GaTe the PL lifetime for localized states is shorter than in GaSe, which may be due to non-radiative escape. Such processes are not included in the model. Another reason could be deviation from the effectively 'ballistic' transport that we assume leads to the carrier escape into regions (1), and its replacement for the larger thicknesses with a slower 'diffusion' process leading to slower non-radiative escape.

Assuming that the measured PL rise-times of ≈20 ps are close to τ_{rel}, we can estimate characteristic non-radiative times τ_{nr1} and τ_{nr2} for several limiting cases. For example for GaSe we obtain the following values using $\tau_{rel}u_1 = 1000$ nm and $\tau_{rel}u_2 = 100$ nm: for $h_{film} = 10$ nm $\tau_{nr1} = 0.05$ ps, for $h_{film} = 30$ nm $\tau_{nr1} = 0.15$ ps, for $h_{film} = 100$ nm $\tau_{nr2} = 7$ ps. For both h_{film} of 10 and 30 nm, the non-radiative decay occurs on a sub-picosecond time-scale. Here, the non-radiative escape is by a factor on the order of 100 faster than relaxation into the light emitting states, which is consistent with a low quantum yield of 10^{-3} reported previously for thin films of MoS_2 [9]. For the middle region of a 100 nm film, the characteristic non-radiative escape time is comparable with the relaxation time into the states giving rise to PL, thus a much higher quantum yield can be expected for films of this thickness.

We also note that in the case of region (2), u_2 should be of the order of a typical thermal velocity of an exciton, v_{th}. By using $T = 10$ K and the exciton mass of 0.1 (or 0.2) [38] of the free electron mass we obtain $\tau_{rel}v_{th} \approx 1200$ (or 900) nm for $\tau_{rel} \approx 20$ ps, very similar to the order of magnitude predicted by the model for the product $\tau_{rel}u_2$.

Note also that the proposed model assumes that the absorption coefficient in the material does not depend on the film thickness. In general, the absorption coefficient may depend on the film thickness if significant changes in the band-structure occur when the film thickness is changed [18, 25]. However, we do not observe significant variation of PL peak energies when the film thickness is reduced. This implies that the changes of the band-structure may be weak, and the absorption coefficient variations may be insignificant. We would expect the

size-quantization (and possibly band-structure modification effects) to become important at film thicknesses of the order of the exciton Bohr radius or the size of localized exciton wavefunction. The weak changes in the PL peak positions observed in our work are possibly related to either small exciton Bohr radius reported to be 3 nm in bulk GaTe [26] and GaSe [39, 40] or relatively strong exciton localization. The (systematic) blue shift in the PL peak position would be expected for film thicknesses of a few nm, which could not be studied systematically here due to weak PL.

3.6. Conclusions

We have investigated thin films of GaTe and GaSe prepared by mechanical exfoliation from bulk crystals, deposited on SiO_2 substrates and capped with a thin layer of Si_3N_4. The study of the optical properties of the thin films has been conducted by means of low-temperature cw and time-resolved micro-PL techniques. The most pronounced property observed is a significant reduction of cw PL intensity by up to 10^5 for thin films of thicknesses about 10 nm compared with films of 150–200 nm. No measurable PL was observed in films thinner than 7 nm. Except for PL decrease, no other clear trends, including size-quantization effects and PL life-time modifications as a function of the film thickness were observed in cw and time-resolved PL. We argue that the reduction of quantum yield occurs due to the non-radiative processes associated with the surface states. The theoretical model that we develop differentiates between the fast non-radiative carrier escape to surface traps in the thin 15–20 nm layers near the film surface, and slower decay in the middle region of the film, where the carriers first move to the surface layers and then decay. The model accounts for the change in the character of the PL decay for thin films with thicknesses less than 30–40 nm, where we expect only fast direct relaxation to surface traps.

We do not refer in our model and interpretation to the direct-to-indirect bandgap transition found for thin InSe films in [18]. The observed strong PL decrease is not accompanied with any significant variation of the PL lifetime, which would most likely accompany such a change in the band structure. This implies that the PL reduction in our case is not associated with this type of transition, and instead the reduction in the radiative recombination contribution is likely due to an increase in the non-radiative decay rate in thin films.

Strong non-radiative decay processes occur in the studied films despite complete encapsulation in Si_3N_4 and SiO_2 providing partial protection of the surface from chemical interactions with the ambient atmosphere. This emphasizes the need for development of novel surface passivation for III–VI films, possibly involving oxygen-free substrates and encapsulation in additional layered materials such as boron nitride. Using these fabrication methods, the large family of III–VI materials may show weaker dependence of quantum yield on film thickness, which will allow them to play an important role as building blocks in van der Waals heterostructures. It is likely that in the near future fabrication of such heterostructures will be carried out in oxygen- and water-free atmospheres and will include carefully designed passivating layers.

Acknowledgments

We acknowledge the financial support of the Graphene Flagship project 604391, FP7 ITN S3NANO, EPSRC grant EP/M012727/1 and Programme Grant EP/J007544/1, SEP-Mexico and CONACYT.

References

[1] Novoselov K S, Geim A K, Morozov S V, Jiang D, Zhang Y, Dubonos S V, Grigorieva I V and Firsov A A 2004 *Science* **306** 666
[2] Novoselov K S, Jiang D, Schedin F, Booth T J, Khotkevich V V, Morozov S V and Geim A K 2005 *Proc. Natl. Acad. Sci.* 102 10451–3
[3] Wang Q H, Kalantar-Zadeh K, Kis A, Coleman J N and Strano M S 2012 *Nat. Nanotechnology* **7** 699–712
[4] Britnell L *et al* 2013 *Science* **340** 1311
[5] Geim A K and Grigorieva I V 2013 *Nature* **499** 419
[6] Radisavljevic D, Radenovic A, Brivio J, Giacometti V and Kis A 2011 *Nat. Nanotechnology* **6** 147
[7] Wu S *et al* 2015 *Nature* **520** 69–72
[8] Withers F *et al* 2015 *Nat. Mater.* **14** 301–6
[9] Mak K, Lee C, Hone J, Shan J and Heinz T 2010 *Phys. Rev. Lett.* **105** 2–5
[10] Splendiani A, Sun L, Zhang Y, Li T, Kim J, Chim C-Y, Galli G and Wang F 2010 *Nano Letters* **10** 1271–5
[11] Eda G, Yamaguchi H, Voiry D, Fujita T, Chen M and Chhowalla M 2011 *Nano Letters* **11** 5111–6
[12] Jones A M *et al* 2013 *Nat. Nanotechnology* **8** 634
[13] Ross J S *et al* 2013 *Nat. Commun.* **4** 1474
[14] Hu P, Wen Z, Wang L, Tan P and Xiao K 2012 *ACS Nano* **6** 5988–94
[15] Late D J, Liu B, Luo J J, Yan A M, Matte H S S R, Grayson M, Rao C N R and Dravid V P 2012 *Adv. Mater.* **24** 3549–54
[16] Liu F, Shimotani H, Shang H, Kanagasekaran T, Zlyomi V, Drummond N, Falko V I and Tanigaki K 2014 *ACS Nano* **8** 752–60
[17] Schwarz S *et al* 2014 *Nano Letters* **14** 7003–8
[18] Mudd G W *et al* 2013 *Adv. Mater.* **25** 5714–8
[19] Lei S D, Ge L H, Liu S, Najmaei Z, Shi G, You G, Lou J, Vajtai R and Ajayan P M 2013 *Nano Letters* **13** 2777–81
[20] Kokh K A, Andreev Y M, Svetlichnyi V A, Lanskii G V and Kokh A E 2011 *Cryst. Res. Technol.* **46** 327–30
[21] Camara M O D, Mauger A and Devos I 2002 *Phys. Rev.* B **65** 125206
[22] Wan J Z, Brebner J L, Leonelli R and Graham J T 1992 *Phys. Rev.* B **46** 1468–71
[23] Hulliger F 1976 *Structural Chemistry of Layer-Type Phases* (Dordrecht: Reidel)
[24] Capozzi V 1981 *Phys. Rev.* B **23** 836–40
[25] Zólyomi V, Drummond N D and Fal'ko V I 2013 *Phys. Rev.* B **87** 195403
[26] Yamamoto A, Syouji A, Goto T, Kulatov E, Ohno K, Kawazoe Y, Uchida K and Miura N 2001 *Phys. Rev.* B **64** 035210

[27] Grasso V, Mondio G, Pirrone M A and Saitta G 1975 Journal of Physics C *Solid State Phys.* **8** 80
[28] Kretinin A V *et al* 2014 *Nano Letters* **14** 3270–6
[29] Kolesnikov N, Borisenko E, Borisenko D and Gartman V 2007 *Journal of Crystal Growth* **300** 294 – 298
[30] Kolesnikov N, Borisenko E, Borisenko D and Bozhko S 2008 *Journal of Crystal Growth* **310** 3287–9
[31] Borisenko E, Kolesnikov N, Borisenko D and Bozhko S 2011 *Journal of Crystal Growth* **316** 20–24
[32] Kolesnikov N, Borisenko E, Borisenko D and Timonina A 2013 *Journal of Crystal Growth* **365** 59–63
[33] Camassel J, Merle P, Mathieu H and Gouskov A 1979 *Phys. Rev.* B **19** 1060–8
[34] Mercier A, Mooser E and Voitchovsky J P 1975 *Phys. Rev.* B **12** 4307–11
[35] Raymond S, Guo X, Merz J L and Fafard S 1999 *Phys. Rev.* B **59** 7624–31
[36] Taylor R A and Rayn J F 1987 Journal of Physics C *Solid State Phys.* **20** 6175
[37] Calarco R, Marso M, Richter T, Aykanat A I, Meijers R, v d Hart A, Stoica T and Lth H 2005 *Nano Letters* **5** 981–4
[38] Watanabe K, Uchida K and Miura N 2003 *Phys. Rev.* B **68** 155312
[39] Mooser E and Schluter M 1973 *Nuovo Cimento* B **18** 164
[40] Chikan V and Kelley D F 2002 *Nano Letters* **2** 141